Journal of Power Sources 203 (2012) 297–301

Contents lists available at SciVerse ScienceDirect

Journal of Power Sources

journal homepage: www.elsevier.com/locate/jpowsour

Short communication

A novel nanocomposite TiO_2 photoanode for highly efficient dye-sensitized solar cells

Wen-Kai Tu[a], Chin-Jung Lin[b], Anindita Chatterjee[a], Guang-Hung Shiau[a,c], Shu-Hua Chien[a,c,*]

[a] Institute of Chemistry, Academia Sinica, Taipei 11529, Taiwan
[b] Department of Environmental Engineering, National I-Lan University, I-Lan 260, Taiwan
[c] Department of Chemistry, National Taiwan University, Taipei 10617, Taiwan

ARTICLE INFO

Article history:
Received 10 June 2011
Accepted 15 November 2011
Available online 25 November 2011

Keywords:
Titanium oxide
Nanotube
Light scattering
Dye-sensitized solar cell

ABSTRACT

In this study, we present a novel trilayered hierarchical TiO_2 nanocomposite film with three different titania, i.e., nanoparticle (NP), submicron particle (SP), and nanotube (NT) for highly efficient dye-sensitized solar cells (DSSCs). The obtained trilayer-structured film exhibits efficient internal light trapping, fast electron transport and fluent redox diffusion. A significant improvement is achieved with a photoenergy conversion efficiency of 9.36% under AM 1.5 G simulated sunlight illumination, corresponding to a ~55% enhancement as compared to that with the same thickness of the NP layer alone.

1. Introduction

Since the first work on dye-sensitized solar cells (DSSCs) was introduced by Grätzel's group in 1991 [1], DSSCs has been considered a potentially efficient device for low-cost renewable energy source. The typical Grätzel's DSSCs based on a nanocrystalline TiO_2 working eletrode with an adsorbed ruthenium-based dye have exhibited good photoenergy conversion efficiency [2,3], whereas the poor utilization of near infrared photons and recombination loss during the photoexcited electrons collection in the random network of TiO_2 nanocrystallines still limit their overall performances [4,5]. To develop more efficient TiO_2 films, intense efforts have been made either to overcome the recombination of photoexcited carriers by replacing a random TiO_2 nanoparticle network with an oriented TiO_2 film [6–8] or to address the generation of photoexcited carriers by adding a light-scattering layer over nanocrystalline TiO_2 film [9–12].

One-dimensional (1D) nanostructures, such as nanorods, nanowires, and nanotubes, featuring highly decreased intercrystalline contacts and charge transport along the oriented axis [7,8], are expected for a higher photoenergy conversion efficiency due to facile electron transport. Tan and Wu [7] constructed a mixed photoanode based on nanoparticle and nanowire, which increased a photoenergy conversion efficiency up to 8.6%. The tubular structure, providing availability of both the internal and external areas of the nanotubes for reaction, has been recognized to be preferable [13]. Recently, we introduced the ground powder of highly crystalline anodic TiO_2 nanotubes as an additive to mix with the nanocrystalline TiO_2 for photoanode film, which improve the light scattering, ion diffusion, and electron transport, thus the performance exceeding 9% [14]. Among the methods for achieving a higher DSSC's efficiency, addition of light-scattering materials has been one of the most effective and practical approach, in which the light-scattering material elongates the path length of incident light within the films, thereby enhancing the light-harvesting capability of the electrode film and the performance [9–12]. Light scattering can be achieved by introducing TiO_2 rough spheres as light-scattering centers [8] or by using a photonic crystal layer as a dielectric mirror [9]. The large TiO_2 particles are normally with relatively low surface area that restricted the dye adsorption capability in the DSSC application and limited the performance. Recently, bifunctional layer has been developed by using the hierarchical-structured layer with hollow TiO_2 microspheres, to offer efficient generation of photo-excited electrons as well as good light-scattering property [15]. However, except for their role in the internal light trapping, these scattering particles hardly offer any additional effect, for instance, the electron transport or the redox penetration. Additionally, these hierarchical structures encounter siginificant challenges when scaled up due to the poor adhesion between layers with large difference in particle size.

In the present work, we successfully constructed two light-scattering layers atop a 12 μm nanoparticle TiO_2 layer as the photoanode for highly efficient DSSCs. The light-scattering

* Corresponding author at: Institute of Chemistry, Academia Sinica, Taipei 11529, Taiwan. Tel.: +886 2 2789 8528; fax: +886 2 2783 1237.
E-mail address: chiensh@gate.sinica.edu.tw (S.-H. Chien).

0378-7753/$ – see front matter © 2011 Elsevier B.V. All rights reserved.
doi:10.1016/j.jpowsour.2011.11.052

layers by mixing the nanotube and submicron particle with TiO_2 nanoparticle, not only improved the cell performance but also indeed performed a much better mechanical strength. Such a trilayered hierarchical TiO_2 nanocomposite electrode showed superior electron-transport property and the light-harvesting efficiency that were confirmed by electrochemical impedance spectroscopy (EIS) and incident photon-to-electron efficiency (IPCE) measurements.

2. Experimental

The TiO_2 nanoparticle (NP) was prepared by the hydrothermal method, in which the titanium tetraisopropoxide was hydrolyzed in 0.1 M $HNO_{3(aq)}$ and then autoclaved at 220 °C for 12 h. After hydrothermal treatment, the white solid was retrieved by centrifugation and dried at 110 °C. The submicron particle (SP) was the commercial anatase TiO_2 from Merck. The TiO_2 nanotube (NT) was synthesized by the alkaline hydrothermal method as described in our previous paper [16,17] using Merck anatase TiO_2 dispersed in 10 M $NaOH_{(aq)}$ and then autoclaved at 130 °C for 96 h. The obtained white precipitate was centrifuged and rinsed with 0.1 M $HNO_{3(aq)}$ until the pH of the eluate reached neutral and was dried at 110 °C overnight.

In this study, all the TiO_2 electrode films were fabricated via printing various TiO_2 pastes onto F-doped SnO_2 (FTO) glass by the doctor blade technique. The pastes were prepared by mixing 100 mg of TiO_2 (i.e., NP, SP, or NT) with 0.67 mL of H_2O and 30 mg of polyethylene glycol (MW = 20,000). The type A electrode film was printed with NP-TiO_2 paste four times to achieve a 12 μm thick film. The bilayer composite-TiO_2 film of type B or C was further printed with a light-scattering layer using the SP-TiO_2 paste (type B) or the NT-TiO_2 paste (type C) atop the 12 μm NP film. Type D is the trilayer electrode film fabricated with two light-scattering layers, printing first the NT-TiO_2 layer on top of a 12 μm NP film and then the SP-TiO_2 layer atop it. Type E is also a trilayer electrode film that used the NP-NT mixture paste and the NP-SP mixture paste for printing the middle and upper layers, respectively, which could be limited the mechanical destruction of the formed layers to a minimal extent. The film was calcined in air at 450 °C for 30 min after each print. Film thickness was monitored by a Dektak-3 surface profiler.

Field emission scanning electron microscopy (FE-SEM) was performed using a JEOL JSM-6500F microscope. High-resolution transmission electron microscopy (HR-TEM) was performed using a JEOL JEM-2011 transmission electron microscope. The crystalline structures were obtained by X-ray diffraction (XRD) on a Siemens D5000 diffractometer equipped with a Cu Kα X-ray source (λ = 1.5405 Å). The Brunauer–Emmett–Teller (BET) surface areas were determined by nitrogen adsorption isotherms at 77 K using a Micromeritics ASAP 2010 Analyzer. The light-scattering property of the TiO_2 films was studied using haze measurement by recording the ultraviolet–visible (UV–vis) spectra on a Hitachi U-3410 UV-vis spectrometer with an integrating sphere.

The DSSCs was constructed as described previously [14,18]. Briefly, the N719-sensitized photoanode was prepared by immersing the TiO_2/FTO (with an active area of 0.25 cm^2) in 0.3 mM $(Bu_4N)_2[Ru(dcbpyH)_2\text{-}(NCS)_2]$ (N719 dye, Solaronix) solution for 24 h for dye adsorption and then further sandwiched with the sputtered-Pt FTO glass, separated by a 25 μm thick hot-melt spacer to assemble the solar cell. The intervening space was filled with liquid electrolytes of 0.5 M LiI, 0.05 M I_2, and 0.5 M tert-butylpyridine in dry acetonitrile. Photocurrent–photovoltage (I–V) characteristics of the DSSCs were measured using an electrochemical analyzer (650B, CH Instruments) under AM 1.5 simulated solar light illumination at an intensity of 100 mW cm^{-2}. The electron impedance spectra of DSSCs were carried out under illumination with AM 1.5 G simulated solar light (100 mW cm^{-2}) at an applied bias of open-circuit voltage (V_{OC}) and alternative signal magnitude of 10 mV in the 10^{-2} to 10^5 Hz frequency range. In the incident photon-to-current conversion efficiency measurements, the light source was a 300 W Xe lamp equipped with an Oriel 74100 monochromator. After these measurments, the adorbed N719 dye on the sensitized film was washed out by 0.2 M NaOH solution. The amount of adsorbed N719 dye ($N719_{ads}$) were then determined by UV–vis spectroscopy.

3. Results and discussion

The FE-SEM images of NP and SP are shown in Fig. 1(a) and (b), respectively. The average particle size of NP was 20 nm, whereas SP was significantly larger at 200 nm. The FE-SEM image of NT prepared by the alkaline hydrothermal method is shown in Fig. 1(c). The length of the randomly tangled nanotube was up to ~200 nm. As shown in the HR-TEM image (the inset of Fig. 1(c)), the outer diameter of the nanotube was ~10 nm and the inner diameter was ~4 nm. The multi-walled nanotubular structure with a wall thickness of ~3 nm was clearly observed. According to the XRD profiles, NP and SP exhibited pure anatase phase while the weak XRD peaks of NT revealed the typical titania nanotubes [17]. The BET surface areas of NP, SP, and NT were 135, 5, and 310 $m^2\ g^{-1}$, respectively. Fig. 1(d) shows the haze measurement of the various TiO_2 films with the same film thickness (L_F) of 12 μm. Haze is defined as the ratio of the diffused transmittance to total optical transmittance, which can specify the extent of light scattering as light passes through a transparent material [19]. The inset figure of Fig. 1(d) shows the optical image of the prepared TiO_2 films coating on the FTO glass. Visually, the NP film is optically transparent, the NT film is translucent, and the SP film is almost opaque. In general, the more opaque the TiO_2 film, the more incident light will be scattered.

The photovoltaic performance parameters of DSSCs based on NP, SP, as well as NT films are summarized in Table 1. Among them, the NP-based cell showed the best photoenergy conversion efficiency (η) of 7.44%, which was much better than that of the NT-based cell (4.27%) and SP-based cell (1.40%). The best photovoltaic performance of NP-based cell was mainly contributed by its much higher short-circuit photocurrent density (I_{SC}) of 16.8 mA cm^{-2}. The I_{SC} values of NT- and SP-based cells were merely 7.7 and 3.0 mA cm^{-2}, respectively. The higher value of I_{SC} was correlated to a higher amount of adsorbed N719 dye. The open-circuit voltage (V_{OC}) of NT-based cell was 805 mV, which was higher as compared with that of NP- and SP-based cells. The higher V_{OC} could be attributed to the lower electron recombination, resulting in an increase in electron transport in the NT film and thus the negative shift of the quasi-Fermi level [20]. Accordingly, NP features high N719 dye adsorption ability. SP shows excellent light-scattering behavior to elongate the path length of the incident light within the device. NT, due to its unique 1D architecture, possesses higher effective electron transport property.

In this study, various TiO_2 nanocomposite electrodes consisting of NP, SP, and NT with hierarchical structures were fabricated as described in the experimental part. The morphology of each electrode was examined by FE-SEM. All types of nanocomposite titania electrodes clearly exhibited hierarchical structures as designed. As can be seen in Fig. 2(a), the FE-SEM images of the type E electrode clearly displayed the trilayer hierarchical TiO_2 morphology. It reveals that the bottom NP layer, the middle NP-NT layer, and the upper NP-SP layer retained the thickness of 12, 5, and 2 μm, respectively. The particle sizes and the mixed phases of the middle and upper layers were clearly distinguished, as can be seen in Fig. 2(b)–(d).

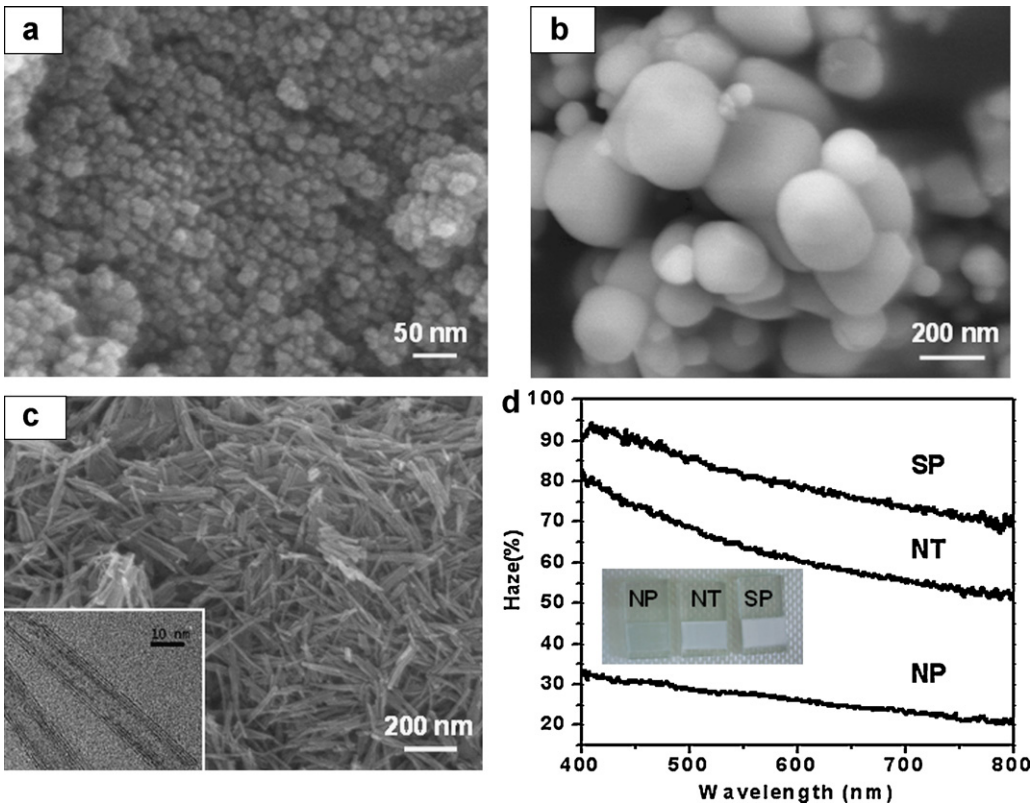

Fig. 1. Physical properties of NP, SP, and NT. FE-SEM images of (a) NP, (b) SP, (c) NT (inset shows the HR-TEM image); and (d) Haze measurement of electrodes based on NP, SP, and NT films (inset shows the image of TiO_2 films).

Table 1
Photovoltaic performance parameters of DSSCs based on NP, SP, and NT films.

TiO_2 films	L_F (μm)	$N719_{ads}$ (μmol cm^{-2})	V_{OC} (mV)	I_{SC} (mA cm^{-2})	FF	η (%)
NP	12	0.100	773	16.8	0.57	7.44
SP	12	0.009	795	3.0	0.59	1.40
NT	12	0.086	805	7.7	0.69	4.27

Table 2
Photovoltaic performance parameters of various hierarchical TiO_2 nanocomposite-based DSSCs.

Electrode type	TiO_2 microstructure	L_F (μm)	$N719_{ads}$ (μmol cm^{-2})	V_{OC} (mV)	I_{SC} (mA cm^{-2})	FF	η (%)
A	NP	12	0.102	773	16.8	0.57	7.44
B	NP/SP	17	0.106	770	18.5	0.56	8.08
C	NP/NT	17	0.129	765	19.4	0.58	8.65
D	NP/NT/SP	19	0.132	745	21.6	0.56	9.04
E	NP/NP-NT/NP-SP	19	0.159	750	22.5	0.55	9.36
F	NP	19	0.154	727	15.0	0.56	6.08

The photovoltaic performance data of DSSCs based on all types of TiO_2 nanocomposite films are summarized in Table 2. The data for the 19 μm thick type F electrode made of pure NP anode are also listed for comparison. Both I_{SC} and η were significantly increased by adding light-scattering layers on top of the NP layer. In the bilayer electrodes, as working for a scattering layer, the NT exhibited a better performance than the SP. The trilayer electrode based DSSC even performed much better. As can be seen from Table 2, the type D exhibited a η of 9.04% that is ~5% increase as compared with the type C. As mixing the NT, as well as the SP, with the NP in the scattering layer, the cell of type E was not only further increased in $N719_{ads}$, along with an enhancement of η, but also exhibited

Table 3
Electron transport properties of various hierarchical TiO_2 nanocomposite-based DSSCs.

Electrode type	TiO_2 microstructure	k_{eff} (s^{-1})	τ (ms)	R_k (Ω)	R_w (Ω)	D_{eff} (cm^2 s^{-1})
A	NP	13.63	73	19.5	1.12	3.4×10^{-4}
B	NP/SP	10.93	92	23.0	4.21	1.7×10^{-4}
C	NP/NT	34.49	29	13.0	1.09	1.2×10^{-3}
D	NP/NT/SP	19.92	50	13.3	0.88	1.1×10^{-3}
E	NP/NP-NT/NP-SP	18.28	55	16.2	1.54	7.0×10^{-4}

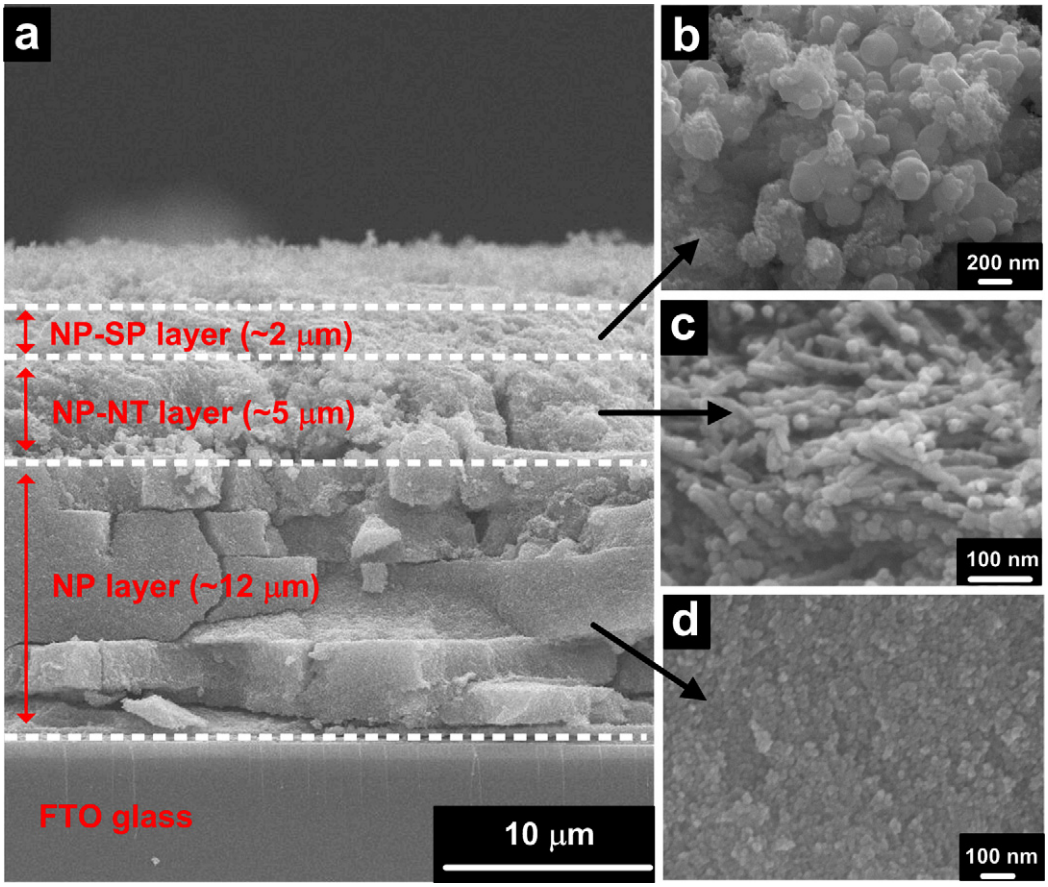

Fig. 2. Cross-sectional FE-SEM image of the trilayer NP/NP-NT/NP-SP electrode (type E); (b) NP-SP layer; (c) NP-NT layer; and (d) NP layer.

the stronger mechanical film-strength. The photoconversion efficiency of 9.36% was achieved, ~55% enhancement as compared to the same thickness of the nanoparticle TiO_2 layer alone. In the hierarchical electrodes, the η increases along with the thicker L_F indicates the addition of NT and SP causes the ease of ion diffusion and electron transport in the mixed films.

The EIS measurements were performed under illumination with AM 1.5 G simulated solar light at an applied bias of V_{OC}. The Nyquist plots of the obtained impedance data are depicted in Fig. 3. The data were fitted in terms of the appropriate equivalent circuit using the Z-VIEW software as described previously [14]. The derived parameters, including the first-order reaction rate constant for the loss of electrons (k_{eff}), the dark reaction impedance (R_k), and the diffusion reaction impedance (R_w) in various TiO_2 nanocomposite films

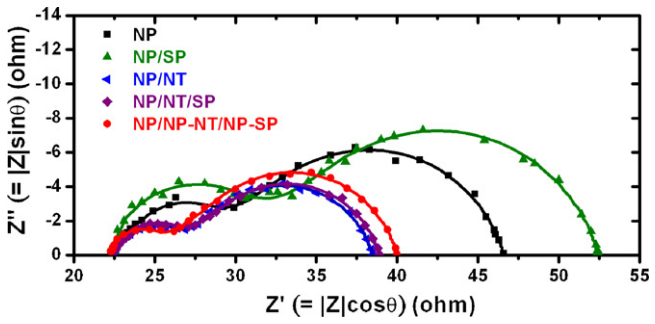

Fig. 3. Nyquist plots of the impedance spectra of DSSCs based on various hierarchical TiO_2 nanocomposite electrodes.

with L_F, are summarized in Table 3. The effective electron diffusion coefficient (D_{eff}) was calculated using Eq. (1) [21].

$$D_{eff} = \left(\frac{R_k}{R_w}\right)(L_F^2 \times k_{eff}) \quad (1)$$

Based on the D_{eff} values of the various nanocomposite TiO_2 electrodes, the contribution to the D_{eff} clearly appeared in the order of NT > SP > NP. The 1D architecture of NT was the best for electron transport. Thus, higher D_{eff} values were obtained for all the cells containing NT in the anode. The enhancement in the electron transport property was one of the major factors in the improvement of the performance of DSSCs.

To determine the effect of light-scattering layers on cell performance, the measured monochromatic IPCE was obtained by normalizing it to the maximum intensity of 520 nm, as shown in Fig. 4. The bilayer electrodes of types B and C showed clear enhancement in the order of C > B > A on the right-hand side (RHS, >520 nm), although the curves on the left-hand side (LHS, <520 nm) appeared irrational. However, the NT was evidently more effective than the SP in light harvesting. The trilayer-based DSSCs of types D and E showed further notable increase in IPCE on the RHS, with type E slightly higher than type D. Moreover, the normalized IPCE of type E was clearly higher than that for type D on the LHS, which is in agreement with the amount of dye adsorption as listed in Table 2. The peak shoulder at ~625 nm was due to the adsorbed N719 dye molecules [4]. The full spectrum enhancement and the maximum light-harvesting efficiency presented for the trilayer-based (NP/NP-NT/NP-SP) cell of type E is evidently due to the enhanced light absorption by the dye adsorbed on the NP and NT on the LHS and the efficient light scattering by the SP and NT on the RHS.

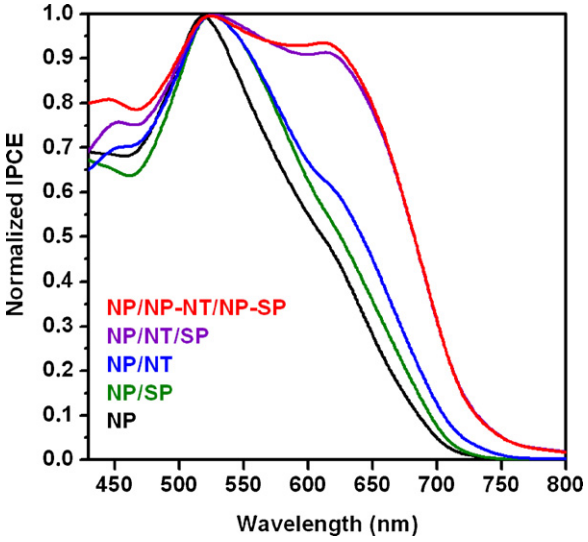

Fig. 4. Monochromatic IPCE of DSSCs based on various hierarchical TiO_2 nanocomposite electrodes.

4. Conclusions

By tailoring the microstructure of a TiO_2 electrode film integrated with the nanoparticle, the nanotube, and the submicron particle, we successfully fabricated highly efficient DSSCs. The type E trilayer electrode film, achieved by mixing the nanotube and submicron particle with TiO_2 nanoparticle in the middle and upper layers, served as a multifunction in terms of higher dye adsorption, stronger mechanical strength, favorable electron transport, effective light scattering, and fluent redox diffusion. A remarkable improvement was achieved with a solar-to-electricity conversion efficiency of 9.36% under AM 1.5 G simulated sunlight illumination, corresponding to a ~55% enhancement compared to the same thickness of the nanoparticle TiO_2 layer alone.

Acknowledgement

We acknowledge the financial supports from Academia Sinica and National Science Council of Taiwan.

References

[1] B. O'Regan, M. Grätzel, Nature 353 (1991) 737.
[2] M. Grätzel, Inorg. Chem. 44 (2005) 6841.
[3] F. Gao, Y. Wang, D. Shi, J. Zhang, M.K. Wang, X.Y. Jing, R. Humphry-Baker, P. Wang, S.M. Zakeeruddin, M. Grätzel, J. Am. Chem. Soc. 130 (2008) 10720.
[4] C.J. Barbé, F. Arendse, P. Comte, M. Jirousek, F. Lenzmann, V. Shklover, M. Grätzel, J. Am. Ceram. Soc. 80 (1997) 3157.
[5] H.J. Snaith, Adv. Funct. Mater. 20 (2010) 13.
[6] M. Wei, Y. Konishi, H. Zhou, H. Sugihara, H. Arakawa, J. Electrochem. Soc. 153 (2006) A1232.
[7] B. Tan, Y.Y. Wu, J. Phys. Chem. B 110 (2006) 15932.
[8] L. Zhao, J.G. Yu, J.J. Fan, P.C. Zhai, S.M. Wang, Electrochem. Commun. 11 (2009) 2052.
[9] S. Nishimura, N. Abrams, B.A. Lewis, L.I. Halaoui, T.E. Mallouk, K.D. Benkstein, J. van de Lagemaat, A.J. Frank, J. Am. Chem. Soc. 125 (2003) 6306.
[10] Z.S. Wang, H. Kawauchi, T. Kashima, H. Arakawa, Coord. Chem. Rev. 248 (2004) 1381.
[11] L. Yang, Y. Lin, J. Jia, X. Xiao, X. Li, X. Zhou, J. Power Sources 182 (2008) 370.
[12] Y. Qui, W. Chen, S. Yang, Angew. Chem. Int. Ed. 49 (2010) 3675.
[13] Y.Q. Wang, Z.D. Wei, B. Gao, X.Q. Qi, L. Li, Q. Zhang, M.R. Xia, J. Power Sources 196 (2011) 1132.
[14] C.J. Lin, W.Y. Yu, S.H. Chien, Appl. Phys. Lett. 91 (2007) 233120.
[15] H.J. Koo, Y.J. Kim, Y.H. Lee, W.I. Lee, K. Kim, N.G. Park, Adv. Mater. 20 (2008) 195.
[16] S.H. Chien, Y.C. Liou, M.C. Kuo, Synth. Method 152 (2005) 333.
[17] K.P. Yu, W.Y. Yu, M.C. Kuo, Y.C. Liou, S.H. Chien, Appl. Catal. B 84 (2008) 112.
[18] C.J. Lin, W.Y. Yu, S.H. Chien, J. Mater. Chem. 20 (2010) 1073.
[19] Y. Chiba, A. Islam, R. Komiya, N. Koide, L.Y. Han, Appl. Phys. Lett. 88 (2006) 223505.
[20] S. Ito, S.M. Zakeeruddin, R. Humphry-Baker, P. Liska, R. Charvet, P. Comte, M.K. Nazeeruddin, P. Péchy, M. Takata, H. Miura, S.M. Uchida, Grätzel, Adv. Mater. 18 (2006) 1202.
[21] M. Adachi, M. Sakamoto, J. Jiu, Y. Ogata, S. Isoda, J. Phys. Chem. B 110 (2006) 13872.